Journal of Porous Materials (2021) 28:1563–1576
https://doi.org/10.1007/s10934-021-01105-0

Synthesis and characterization of cobalt nanoparticles containing anionic polymer hydrogel nanocomposite catalysts for fast reduction of nitrocompounds in water

Nusrat Jabeen[1] · Zahoor H. Farooqi[2] · Attaullah Shah[3] · Abid Ali[4] · Muhammad Khurram[5] · Khalid Mahmood[6] · Nurettin Sahiner[7] · Muhammad Ajmal[8]

Accepted: 7 June 2021 / Published online: 15 June 2021

Abstract

Design and development of hydrogel based metal nanocomposites is of vital significance in the field of industrial waste management. In this study, the synthesis of poly (N-isopropylacrylamide-co-2-Acrylamido-2-methylpropane sulfonic acid) hydrogel and embedment of cobalt nanoparticles in the prepared hydrogel was demonstrated followed by the evaluation of catalytic potential of the as-prepared cobalt nanoparticles-hydrogel nanocomposite. The prepared hydrogel and corresponding nanocomposite were characterized by Fourier Transform Infrared (FTIR) spectroscopy to identify functional groups, Energy Dispersive X-ray (EDX) and Inductively Coupled Plasma—Optical Emission Spectrometry (ICP-OES) analysis to confirm the presence of cobalt, and Transmission Electron Microscopy (TEM) to assess the spatial morphology of cobalt nanoparticles. The prepared hydrogel showed absorption of water via non-Fickian mechanism, resulting in swelling as much as 69 times of its dry weight. The nanoparticles were found to be spherical in shape and having diameters around 25 nm. The potential catalytic properties of the cobalt nanoparticles-hydrogel nanocomposite were assessed while reducing 4-nitrophenol, 2-nitrophenol, 4-nitroaniline, and 2-nitroaniline to their corresponding amino compounds. The catalytic reactions were performed under varying temperatures and catalyst quantities, besides the catalyst was also subjected to rigorous repeated usage to evaluate its recycling potential. The thermodynamic parameters such as activation energy, activation entropy change, and activation enthalpy change were also calculated. The catalyst was found to be more effective in reducing 4-nitrophenol with a maximum rate constant of 4.67 min^{-1}. A gradual decline in catalytic reduction rate was observed when the same catalyst was repeatedly used for five consecutive cycles.

Keywords Hydrogels · Nanocomposites · Catalysis · Activation Energy

✉ Muhammad Ajmal
m.ajmal65@yahoo.com

[1] Department of Chemistry, University of Wah, Wah Cantt, Pakistan

[2] School of Chemistry, University of the Punjab, Lahore, Pakistan

[3] National Institute of Laser & Optronics-College (NILOP-C), PIEAS Islamabad,, P.O Nilore, Islamabad, Pakistan

[4] Department of Chemistry, University of Lahore, Lahore, Pakistan

[5] Department of Chemistry, Tsinghua University, Beijing, China

[6] Institute of Chemical Sciences, Bahauddin Zakariya University, Multan, Pakistan

[7] Faculty of Science and Arts, Chemistry Department, Canakkale Onsekiz Mart University, Terzioglu Campus, 17100 Canakkale, Turkey

[8] Department of Chemistry, University of Education, Attock Campus, Attock 43600, Pakistan

1 Introduction

Life owes its existence to catalysts [1]. A variety of products in today's world, ranging from fuels, foodstuff, fertilizers, pharmaceuticals, insecticides, and fungicides etc., are available in bulk because of catalysts [2]. Highly toxic aromatic nitro compounds are essential components of chemical reactions occurring in industrial processes, consequently we find them in residual effluents in significant concentration that pose serious environmental threat to living organisms if kept untreated [3]. Catalytic reduction is a green method not only to remove these harmful chemicals from industrial effluents but to produce anilines; precursors to many useful chemical reactions [4]. A catalyst with high efficiency and stability have always been the main area of research for material scientist and technologists. Nanomaterials, since their recognition by Richard Feynman, have gained much importance as catalysts because of the confinement of electronic motion in a nanometre regime that leads to an exceptional catalytic activity [5]. Metal nanoparticles, owing to their extraordinary surface energies and high surface to volume ratios, tend to agglomerate, thus degrading their catalytic efficiencies [6]. Hence, to maintain their outstanding catalytic properties with uniform distribution, various kinds of support materials have been used. Silica [7, 8], block co-polymer micelles [9, 10], dendrimers [6, 11, 12], polymer brushes [13] etc. are few examples of support materials. However, many researchers have focused on hydrogels as a support materials for nanoparticles mainly because of their tunable characteristics and stimuli responsive nature that provide with great flexibility and control over the size and shape of metal nanocatalysts [14–19]. The hydrogels swell to a large extent in water thus acting as excellent mediums for catalytic reactions occurring in aquatic media. A range of available functional groups e.g. $–SO_3H$, –OH, $–NH_2$, –COOH and –SH induce a variety of desired properties and facilitate metal uptake due to electrostatic interaction between metal ions and the functional groups [20–22]. Their crosslinked network limits the movement of nanoparticles hence impart them with long term catalytic activity, storage stability, and handy recycling procedures like filtration and centrifugation [21].

Metal nanoparticles loaded hydrogel proves to be an efficient catalytic system with a variety of advantages. It combines the merits of stability, accessibility and ease of separation which are characteristics of heterogeneous catalysis [23]. It also unites macroscopic stimuli responsive behaviour with quantum sized effects of nanoparticles. These are novel materials merging organic and inorganic regimes thus giving rise to a multidisciplinary field for modern research. High surface area and energy make metal nanoparticles promising materials for catalysis. Owning to the ease of metal ions incorporation and their subsequent chemical reduction, many metal nanoparticles loaded polymeric hydrogel systems have been investigated for their catalytic behaviour in reducing organic pollutants e.g., aromatic nitro compounds. Many researchers incorporated precious metals like Au [24–28], Ag [4, 29–33], Pt [34, 35], and Pd [36] in hydrogels and subsequently applied them to reduce aromatic pollutants and reported satisfactory results regarding their catalytic efficiency and stability. However, research trends are now being averted to less expensive and easily available transition metals to develop low cost and economical ways to process on industrial scales. The main drawback of replacing precious metals with low-cost transition metals is subsequent reduction in catalytic activity and stability. To improve the catalytic efficiency of metal nanoparticles, it may be hypothesized that metal nanoparticles with suitable particle size, stability, and easily approachable surface for the reactants to get adsorbed are the appropriate parameters. These parameters can be controlled by fabricating metal nanoparticles in hydrogels of suitable chemical composition and appropriate mesh sizes. Poly(N-isopropylacrylamide) (PNIPAM) has been extensively utilized to form hydrogels due to its solubility in water and ease of synthesis by a simple free radical polymerization method [3, 37]. To enhance the swelling and the capacity of metal ion absorption, NIPAM has been copolymerized with some hydrophilic monomers having metal ion absorbing tendencies such as acrylic acid [32], methacrylic acid [38–40], allyl acetic acid [41], etc. Likewise, 2-acrylamido-2-methyl-propanosulfonic acid (AMPS) monomer has greater swelling tendency as compared to acrylates and can be copolymerized with NIPAM by simple free radical polymerization. Relatively higher swelling capacity of poly (N-isopropylacrylamide-co-2-acrylamido-2-methyl-propanosulfonic acid) [p(NIPAM-co-AMPS)] hydrogel can provide fast diffusion of reactants towards the incorporated metal nanoparticles which actually act as catalyst. In this context, the current work was designed to explore the potential of p(NIPAM-co-AMPS) bulk hydrogel in the fabrication of metal nanoparticles and subsequently as reactor media and catalyst in catalytic reactions. NIPAM was copolymerized with AMPS in equal mole ratios by free radical polymerization to prepare p(NIPAM-co-AMPS) bulk hydrogel. Cobalt nanoparticles were prepared in the p(NIPAM-co-AMPS) bulk hydrogel by in-situ chemical reduction of cobalt (II) ions, loaded by immersing the hydrogel in Co (II) aqueous solution. The cobalt nanoparticles loaded p(NIPAM-co-AMPS) bulk hydrogel [Co-p(NIPAM-co-AMPS)] was employed as a catalyst to accomplish the chemical reduction of 4-nitrophenol (4-NP), 2-nitrophenol (2-NP), 4-nitroaniline (4-NA) and 2-nitroaniline (2-NA).

The activation parameters like activation energies and enthalpy changes were also calculated to ascertain the effect of temperature on catalytic efficiency. The catalytic system was also examined for its stability and potential of recycling.

2 Experimental

2.1 Materials

The monomers used in this work were N-isopropyl acrylamide (NIPAM, 97%, Merk) and 2-acrylamido-2-methyl propane sulfonic acid (AMPS, 99%, Merk). Cross linking agent *N, N*–methylenebisacrylamide (MBA, 99%, Panreac), initiator ammonium persulfate (APS, 97%, Riedel) and accelerator N,N,N′,N′ tetramethylethylenediamine (TEMED, 99%, VWR) were used to carry out free radical polymerization. Cobalt (II) chloride hexahydrate ($CoCl_2.6H_2O$, 98% Sigma Aldrich) was used as water soluble metal ion precursor. In order to reduce cobalt ions to cobalt nanoparticles and nitro compounds to amino compounds, sodium borohydride ($NaBH_4$, 98% Uni-Chem) was applied as a reducing agent. To perform catalytic tests, 4-nitrophenol (4-NP, Uni-Chem), 2-nitrophenol (2-NP, Uni-Chem), 2-nitroaniline (2-NA), and 4-nitroaniline (4-NA, Uni Chem) was used as reactant. All chemicals were used as received, without any prior modification. Deionized water was used as solvent and reaction medium throughout these experiments.

2.2 Synthesis of p(NIPAM-co-AMPS) hydrogel

Synthesis of p(NIPAM-co-AMPS) hydrogel was carried out via free radical polymerization, with equal mole ratios of both the monomers. Both the NIPAM and AMPS were dissolved in deionized water separately to obtain their clear solutions. The aqueous solutions of both the monomers were mixed. The mixture was stirred to obtain a clear solution again. To this mixture, MBA (1 mol% of both the monomers) and APS (1 mol% of both the monomers) were added as a crosslinking agent and initiator, respectively. Polymerization reaction was caused to initiate by adding 200 µL of TEMED, thereafter. The resulting transparent solution was then transferred to plastic straws and kept as such for 24 h at ambient temperature. Hydrogel thus formed, was drawn out of straws and immersed in deionized water to wash out the unreacted species and other impurities. For this washing, the pieces of hydrogel were kept submersed in deionized water for five days, filtering and replenishing water twice a day. Washed hydrogel was then filtered and dried at 70 °C till constant weight. The dried hydrogel was subsequently used for the characterization and synthesis of cobalt nanoparticles.

2.3 Synthesis of Co-p(NIPAM-co-AMPS) hydrogel

Poly (NIPAM-co-AMPS) dried hydrogel was immersed in aqueous solution of cobalt (II) chloride having concentration of 1000 ppm w.r.t Co (II) ions and stirred continually for 24 h at 30 °C. The metal ions loaded hydrogel was then filtered and washed with deionized water to remove loosely bound metal ions. Cobalt ions loaded in the hydrogel were reduced by treating with freshly prepared 0.1 M aqueous solution of $NaBH_4$ in a beaker for half an hour. The obtained Co-p(NIPAM-co-AMPS) hydrogel was then filtered out, washed, and dried completely at 70 °C.

2.4 Characterization

The amount of cobalt in Co-p(NIPAM-co-AMPS) hydrogel was determined using inductively coupled plasma-optical emission spectrophotometer (ICP-OES) using Thermoscientific iCAP-6500 model. For this purpose, Co-p(NIPAM-co-AMPS) hydrogel was immersed in concentrated HCl for 24 h. A sample was withdrawn from this solution, diluted and then analysed with ICP-OES spectrophotometer. Thermogravimetric study (TGA) was carried out by using Mettler Toledo TGA/DSC-2 in the temperature range 25–800 °C. The sample were analysed in nitrogen environment (flow rate 100 ml/minute and temperature ramp of 10 °C/min). Composition of Co-p(NIPAM-co-AMPS) hydrogel was studied using Bruker Alpha II Fourier Transform Infra-Red (FTIR) spectrophotometer and Energy Dispersive X-ray (EDX) spectroscopy with Octane Elite EDAX analyser. X-ray diffractometer (XRD) patterns of hydrogel and its nanocomposites were obtained with PANalytical X'pert XRD having Cu Kα radiation source ($\lambda = 1.54$ Å) at 40 kV and 40 mA. Scans were collected from $2\theta = 5°$ to 70°. Catalytic parameters for the Co-p(AMPS-co-NIPAM) hydrogel were evaluated by Ultraviolet Visible (UV/Vis) spectroscopy using SPECORD 200 PLUS – 223E1156F.

2.5 Hydrogel swelling studies

Swelling of p(NIPAM-co-AMPS) hydrogel was studied by immersing a completely dried cylindrical piece of hydrogel in 500 ml deionized water at 25 °C. After 15 min, the piece of hydrogel was taken out. Excess water on the surface was wiped out with tissue paper, weighed, and then placed back to the same deionized water. In this way, increasing weight of the hydrogel was measured at regular time intervals till a constant weight was attained for the fully swollen p(NIPAM-co-AMPS) hydrogel. Equilibrium swelling ratio (ESR) was determined by the Eq. (1).

$$ESR = \frac{W_s - W_d}{W_d} \quad (1)$$

where, W_s = weight of swollen gel
W_d = weight of dried gel.

2.6 Catalytic applications

Catalytic properties of Co-p(NIPAM-co-AMPS) hydrogel were explored in the reduction of 4-nitrophenol (4-NP), 2-nitrophenol (2-NP), 4-nitroaniline (4-NA) and 2-nitroaniline (2-NA) carried out by excess of $NaBH_4$ at different temperatures. For this purpose, 0.0025 M 4-NA, 0.005 M 2-NA, 0.01 M 4-NP and 2-NP solutions were prepared. To the aliquot of 50 ml from each of these solutions, 0.756 g of $NaBH_4$ was mixed and continued to stir at ambient temperature in the presence of 0.03 g of Co-p(NIPAM-co-AMPS) hydrogel containing to 2 mmol of Co-catalyst as determined by ICP-OES. The progress of the reaction was tracked with VU-Vis spectrophotometer at regular intervals by withdrawing samples of 0.5 ml and diluting with deionized water. Absorption of nitro compounds was analysed at their respective λ_{max}, that is 380 nm for 4-NA, 414 nm for 2-NA, 400 nm for 4-NP and 415 nm for 2-NP. Decrease in the absorption of each nitro compound at its corresponding λ_{max} with time was a clear indication of the catalyst at work. In order to study the effect of temperature and to evaluate their activation constants, the reactions were conducted at different temperatures in the temperature window of 20–63 °C for each of nitro compounds mentioned above. Recycling of the catalyst was performed at room temperature for five consecutive cycles. At the end of each reaction, the catalyst was recovered from the reaction mixture by filtration through plankton cloth filter paper and washed with deionized water. The recovered catalyst was used again for the same reaction under the same set of reaction conditions.

3 Results and discussions

3.1 Synthesis of bare and composite hydrogel

N-isopropylacrylamide monomer was copolymerized with 2-acrylamido-2-methylpropane sulfonic acid via free radical polymerization reaction using APS as initiator, TEMED as an accelerator, MBA as a crosslinker and deionized water as a solvent. Equal mole ratios (1:1) of both the NIPAM and AMPS were used in the polymerization reaction. In this polymerization reaction, TEMED catalyse the splitting of APS into free radicals which subsequently attack C=C double bond present in AMPS and NIPAM monomers thus causing them to copolymerize in the presence of MBA crosslinker. The resultant hydrogel was soft and elastic in swollen state while it became hard on drying. Poly (NIPAM-co-AMPS) hydrogel contains COO^- and SO_3^{-2} groups, therefore, when it was immersed in aqueous medium containing Co (II) ions the metal ions were absorbed and entangled in the hydrogel due to electrostatic attraction as shown in Fig. 1. The higher osmotic pressure in the surrounding metal solution also drives cobalt ions into the hydrogel network. Since Co (II) ions impart pink colour to the aqueous medium, the colour of Co^{2+} ions loaded hydrogel was also turned to pinkish as can be seen from digital camera image (1) in Fig. 1. This change in colour was an indication of

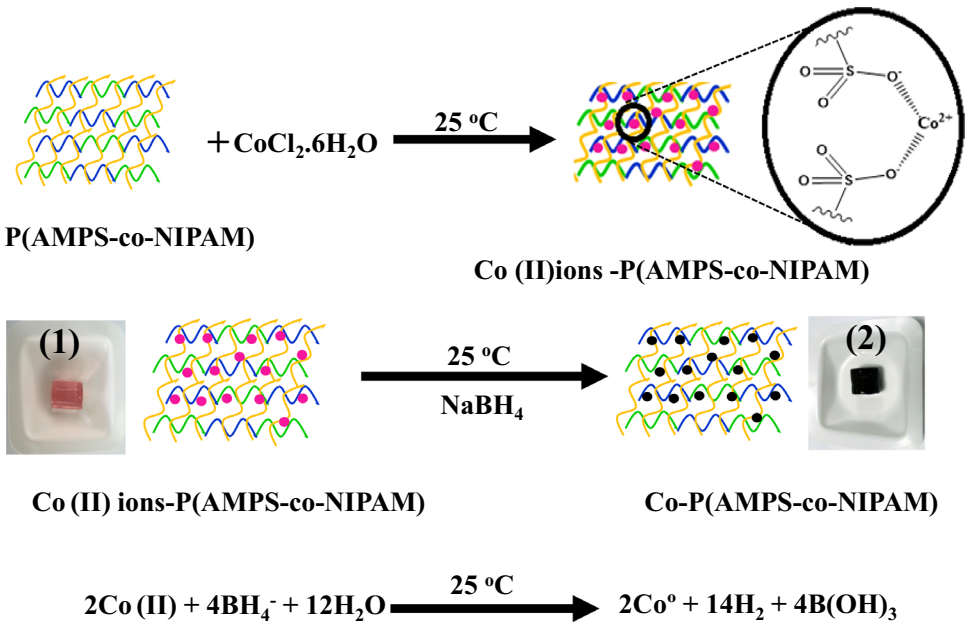

Fig. 1 Schematic representation for the synthesis of Co nanoparticles in p(NIPAM-co-AMPS) hydrogel and corresponding chemical reaction

the entanglement of Co (II) ions in p(NIPAM-co-AMPS) hydrogel. The loaded metal ions were then reduced to the zero valent metal atoms when treated with excess of sodium borohydride in aqueous medium as shown in the chemical reaction given in Fig. 1. After the formation of cobalt nanoparticles, the hydrogel changed its colour from pink to dark black as shown by camera image (2) in Fig. 1. This was the visual indication of immobilization of cobalt nanoparticles in the p(NIPAM-co-AMPS) hydrogel web. Functional groups present in polymer network are not only responsible for metal ions adsorption and uptake, but they are also important for stabilizing the metal nanoparticles inside the network [42]. Metal-ion uptake mechanism depends on the nature of interacting components i.e., metal ion and hydrogel functional groups. P(NIPAM) contains both the hydrophilic (amide) and hydrophobic (isopropyl) functional groups and, therefore, has relatively poor tendency towards metal ions. However, by copolymerizing it with amphiphilic and ionic monomer like AMPS, its metal ions uptake tendency can be improved. Therefore, we prepared p(NIPAM-co-AMPS) hydrogel with reasonable tendency towards Co (II) ions due to presence of amide and sulfonic acid groups.

3.2 FTIR analysis

FTIR spectra of p(NIPAM-co-AMPS) hydrogel and its corresponding nanocomposite with cobalt nanoparticles are shown in Fig. 2a, b, respectively. The compositions and interaction of metal nanoparticles with polymeric functional groups were analysed from these spectra. It is evident from the FTIR spectra that peaks representing C=C and =C–H at ~ 1620 cm^{-1} and just above 3000 cm^{-1} respectively which are present in monomers but absent in both bare and hybrid hydrogel. Absence of these functional groups confirm that all monomers have reacted to form polymer. It is evident from the data that characteristic peak of amide group has shifted its position from 1638 cm^{-1} in bare hydrogel to 1643 cm^{-1} in hybrid gel system. Same is the case for sulfonic acid group. Asymmetric stretch of –S=O is shifted from 1175 cm^{-1} to 1182 cm^{-1}, while symmetric stretch has gone from 1034 cm^{-1} to 1039 cm^{-1}. This peak shifting for some functional groups can be attributed to the engagement of oxygen atom of amide and sulfonic acid group with metal nanoparticles through charge transfer interactions [43]. These forces of attraction play their role in stabilizing metal nanoparticles inside the hydrogel network even when it is in fully swollen state [42]. A broad peak of N–H stretch, appeared at 3292 cm^{-1} and 3295 cm^{-1} in bare and composite hydrogel respectively, indicates the presence of hydrogen bonds with the trapped water molecules and hence hydrophilic character of the prepared hydrogel [43].

3.3 Swelling behaviour in deionized water

A known amount of dried p(NIPAM-co-AMPS) hydrogel was immersed in deionized water and its weight was recorded after definite intervals of time for 72 h. The observed swelling behaviour is demonstrated in Fig. 3a in terms of swelling ratio as a function of time. The digital camera images of the dried and swollen hydrogel clearly represent a significant increase in the volume of hydrogel piece subjected under examination. As evident from Fig. 3a, the equilibrium swelling of the p(NIPAM-co-AMPS) hydrogel in deionized water was attained in 9.5 h. Initial 60% of water uptake data is fitted by the Eq. (2).

$$\ln\left(\frac{M_t}{M_\infty}\right) = \ln k + n \ln t \tag{2}$$

where k is a constant and n represents diffusional exponent, M_t is mass of water absorbed at time t, while M_∞ is the mass of water absorbed at equilibrium swelling. Diffusional exponent 'n' characterises diffusion process occurring within the hydrogel immersed in water. If $n < 0.5$, the diffusion occurs via Fickian mechanism that is only controlled by the concentration gradient. The value of $0.5 < n < 1.0$ symbolises a mechanism that is jointly governed by concentration gradient as well as the chain relaxation processes occurring within the polymer hydrogel during swelling. Swelling is only dependent on chain relaxation processes if diffusional exponent is greater than 1.0 [44]. The value of diffusional exponent calculated from the slope of the straight line of Eq. (2), for initial 60% of swelling data, came out to be 0.54 that depicts non-Fickian mechanism of mass transport inside the gel.

3.4 XRD analysis

The diffraction patterns of the bare p(NIPAM-co-AMPS) hydrogel and its composite with cobalt nanoparticles are shown in the Fig. 3b. Both the bare and composite hydrogel exhibited amorphous structure as no sharp peak was observed in their XRD patterns. The broad peak with its centre at $2\theta = 22°$ is associated with the amorphous phase of p(NIPAM-co-AMPS) [45]. Diffraction pattern of Co-p(NIPAM-co-AMPS) composite hydrogel in contrast with the bare hydrogel as depicted from the Fig. 3b shows the appearance of new peaks that indicates the presence of a new embedded phase different from that of polymeric phase. This metallic phase obviously consists of cobalt nanoparticles which has been confirmed from TEM, EDX and ICP-OES analysis. The sharpness of peaks corresponding to discontinuous metallic phase of cobalt nanoparticles seem to get

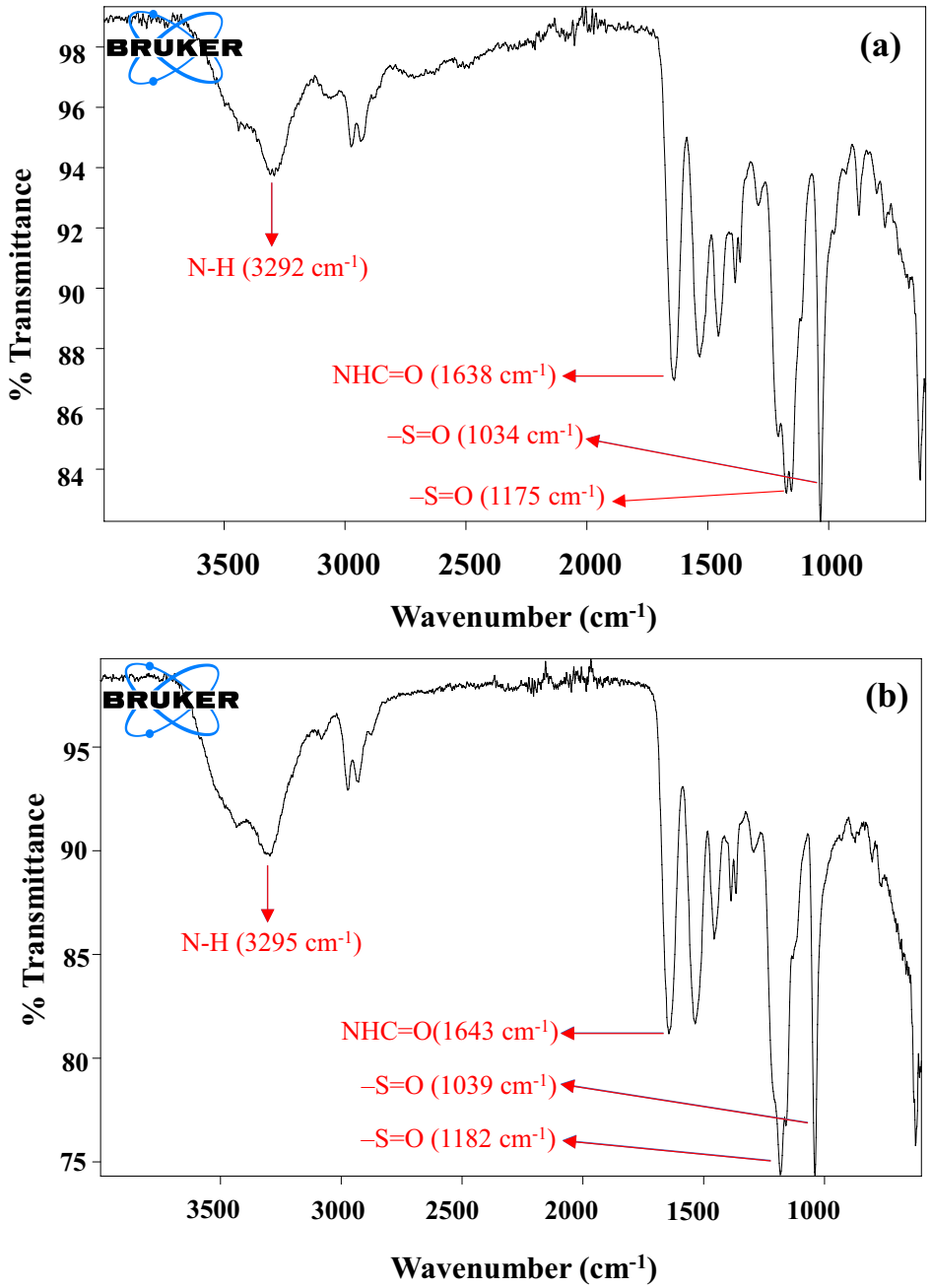

Fig. 2 FTIR spectra of **a** p(NIPAM-co-AMPS) hydrogel and **b** Co-p(NIPAM-co-AMPS) nanocomposite

suppressed by the continuous amorphous phase of the hydrogel which is present in a massive amount [46]. As a consequence of phase suppression, no sharp peak corresponding to cobalt nanoparticles was appeared in the XRD spectrum of composite hydrogel.

3.5 TEM analysis

TEM provided us with pictorial evidence of shape, size and distribution of cobalt nanoparticles embedded in the hydrogel matrix as given in the Fig. 4a. It is clear from the TEM image that there is no aggregation of metal contents reflecting that our prepared p(NIPAM-co-AMPS) hydrogel matrix successfully held cobalt nanoparticles inside its meshes, thus acting as a reactor for the synthesis of nanoparticles as well as stabilizer. Although maximum particle size calculated from the image was 48 nm, most of the nanoparticles were having diameters around 25 nm and appear to be almost spherical in shape. In the preparation of metal nanoparticles in hydrogels, the precursor metal ions are loaded in the meshes of hydrogel network. The mesh size and amount of the functional groups along with

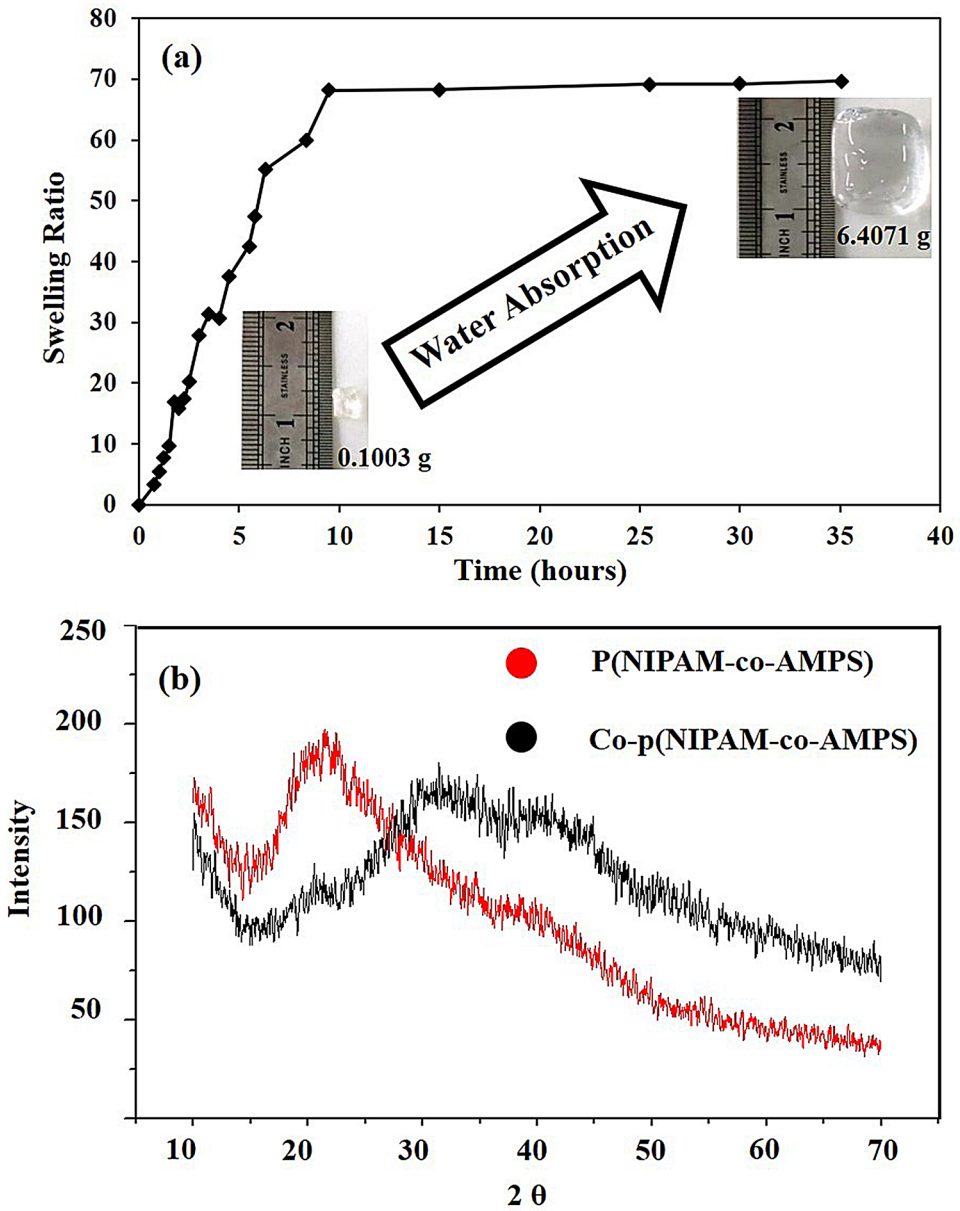

Fig. 3 **a** Swelling ratio of p(NIPAM-co-AMPS) as a function of time. **b** XRD patterns of dried p(NIPAM-co-AMPS) hydrogel and Co-p(NIPAM-co-AMPS) nanocomposite

their chemical nature are responsible for the amount of precursor metal ions loaded within a mesh. The amount of precursor metal ions within a mesh is further responsible for the size of corresponding nanoparticle while its shape depends on the nature and number of functional groups within a mesh. So, the homogeneity in shape and uniform size distribution of the metal nanoparticles prepared in hydrogel network depends on homogeneity in mesh sizes and number of functional groups in each mesh. The homogenous shape and homogeneous sizes of the cobalt nanoparticles depicted from the TEM image represent that p(NIPAM-co-AMPS) hydrogel was prepared with uniform mesh sizes as well as uniform distribution of functional groups.

3.6 ICP-OES and EDX analysis

Cobalt metal contents embedded in the hydrogel were determined with ICP-OES analysis. Co-p(NIPAM-co-AMPS) hydrogel was immersed in the concentrated solution of HCl under constant stirring overnight. The resulting mixture was then diluted and analysed for cobalt contents. ICP-OES analysis have shown that p(NIPAM-co-AMPS) hydrogel adsorbed 120 mg/g of dried gel. Presence of Cobalt nanoparticles embedded in the hydrogel was further confirmed by Energy Dispersive X-Ray (EDX) analysis. Corresponding spectrum is shown in Fig. 4b which shows the presence of carbon, nitrogen, sulphur, oxygen atoms of monomers as well as cobalt atoms of nanoparticles.

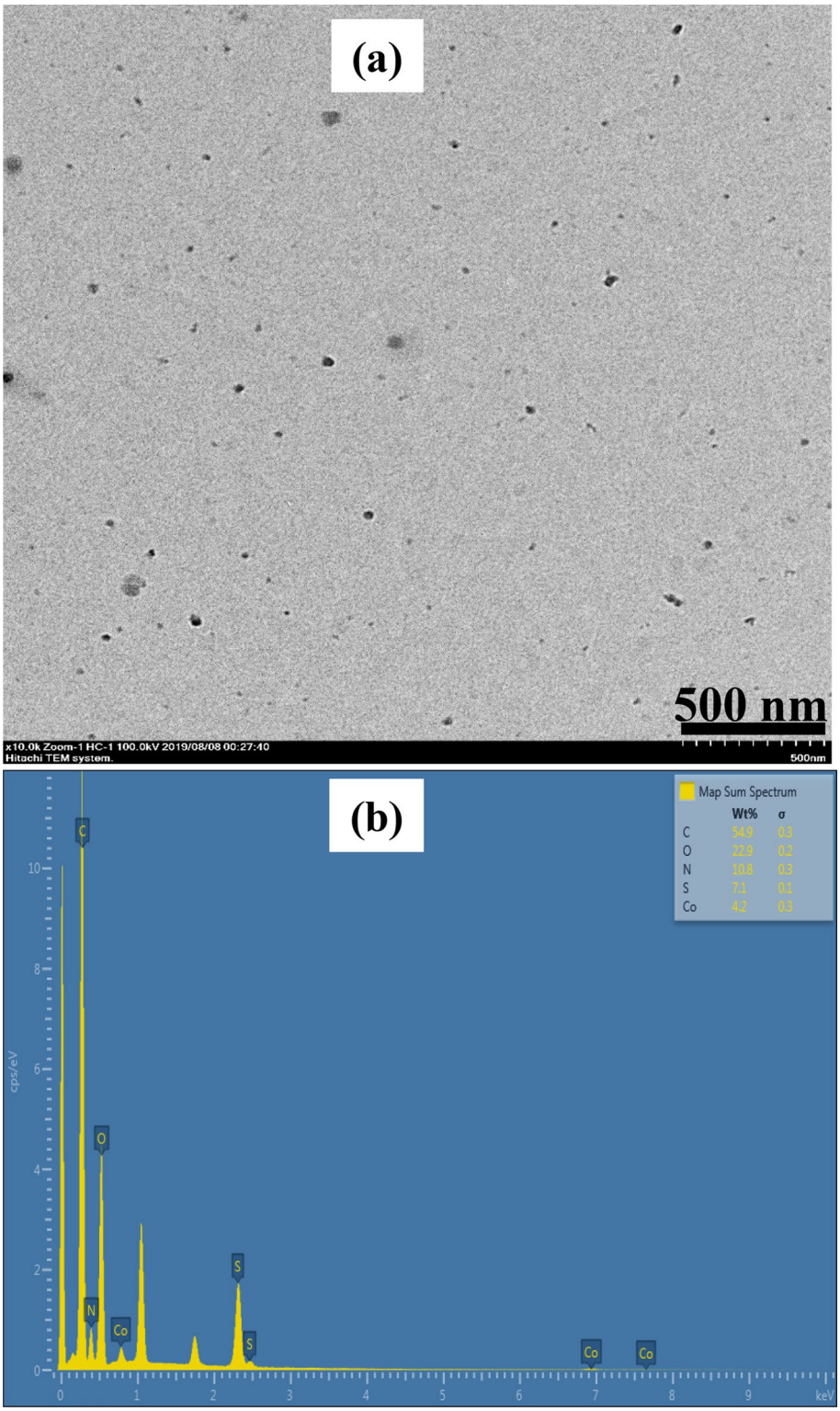

Fig. 4 **a** TEM image of Co-p(NIPAM-co-AMPS) nanocomposite **b** EDX spectrum of Co-p(NIPAM-co-AMPS) nanocomposite

3.7 TGA analysis

TGA analysis of bare and composite hydrogel, revealed that incorporation of nanoparticles in hydrogel resulted in a system that is comparatively robust and stable thermally. Thermogram of p(NIPAM-co-AMPS) hydrogel is given in the Fig. 5a. It can be seen from thermogram that weight loss occurs in three steps over the temperature range of 0–750 °C. In the first step, decline in weight begins at 40 °C and continues till 150 °C. This portion of thermogram represents

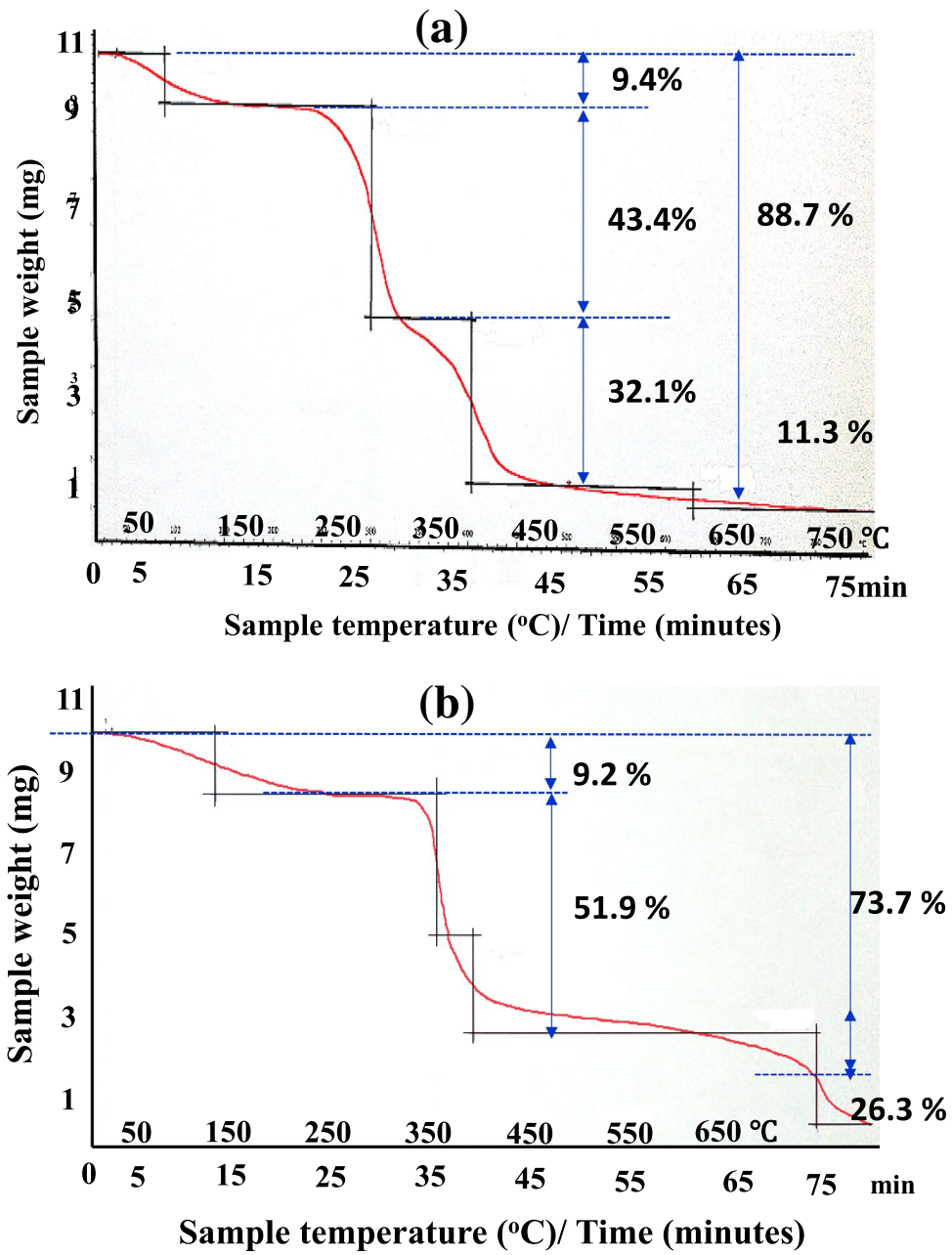

Fig. 5 TGA thermogram of **a** p(NIPAM-co-AMPS) hydrogel and **b** Co-p(NIPAM-co-AMPS) nanocomposite

the loss of free and hydrogen bound water molecules from the hydrogel. Maximum rate of dehydration was observed between 60–100 °C. Beyond 250 °C partial degradation of polymer components occurred. The region from 350–500 °C was characterized by the complete breakdown of polymer components that involve –C–C– chain degradation. There is 11.3% of residue left behind at 750 °C that mainly composed of carbon. Thermogram of Co-p(NIPAM-co-AMPS) hydrogel composite is given in the Fig. 5b. For all the degradation steps of Co-p(NIPAM-co-AMPS) hydrogel composite a clear increment in onset temperatures as compared to p(NIPAM-co-AMPS) hydrogel was observed. This observation is due to the fact that metal nanoparticles coordinate with functional groups of hydrogel, thereby increasing the crosslink density as compared to bare hydrogel which, in turn, increases the thermal stability [47]. So, the TGA data supports the fact of incorporation of metal nanoparticles in the hydrogel.

3.8 Catalytic studies

The prepared Co-p(NIPAM-co-AMPS) hydrogel nanocomposite was applied as catalyst to reduce 4-NP, 4-NA 2-NP, and 2-NA. These nitro compounds are actively employed in various industries e.g., darkening of leather, dyes, paint, colouring, drugs, fungicides etc. and are mostly encountered

in effluents [48, 49]. Detoxifying these harmful chemicals is a major concern for environmental agencies now-a-days. The reduction process of these nitro compounds yields useful amino products. Moreover, the process of reduction can be easily visualized by UV/Vis spectroscopy. It is an experimentally established fact that even using the excess $NaBH_4$ does not make the reduction of nitro compounds to proceed at an appreciable rate for the transfer of electron is strongly hindered by the presence of huge potential barrier between the electron donor specie; BH_4^- and the acceptor nitrophenol. However, a small amount of catalyst lowers the energy hill, and makes the reaction to proceed at ambient conditions with considerable reaction rates [50]. Upon the addition of $NaBH_4$ in the aqueous solution of 4-NP, a shift in absorption maximum from 317 to 400 nm was observed due to the formation of phenolate ion [24, 51] and no significant decrease in the height of absorption peak at 400 nm occurred. Similar observations have also been reported earlier by our research group [49, 52, 53]. When Co-p(NIPAM-co-AMPS) hydrogel composite was added as catalyst, the reaction showed progress at an appreciable pace as depicted from the decrease in the absorbance as a function of time at λ_{max} of phenolate ion. Figure 6a illustrates the decrease in the absorbance of phenolate ion as a function of time. The catalytic potential of Co-p(NIPAM-co-AMPS) hydrogel composite to reduce 2-NP, 2-NA, and 4-NA was also evaluated in the same way. Figure 6b–d represents the decrease in the absorbance of 2-NP, 2-NA, and 4-NA, respectively, during catalytic reduction.

Being in excess, the concentration of $NaBH_4$ does not apparently govern the rates of the reactions [54]. Therefore, pseudo first order kinetics (Eq. 3) was applied on the experimental data for the calculation of the apparent rate constant k_{app}.

$$\ln \frac{C_t}{C_o} = -k_{app} t \tag{3}$$

where, C_t = concentration of nitro compounds at any time t. C_o = initial concentration. k_{app} = Apparent rate constant for pseudo first order reaction.

The concentration is directly related to the absorbance for UV/Vis active species and absorbance is convenient to measure by using UV/Vis spectrophotometer, therefore for

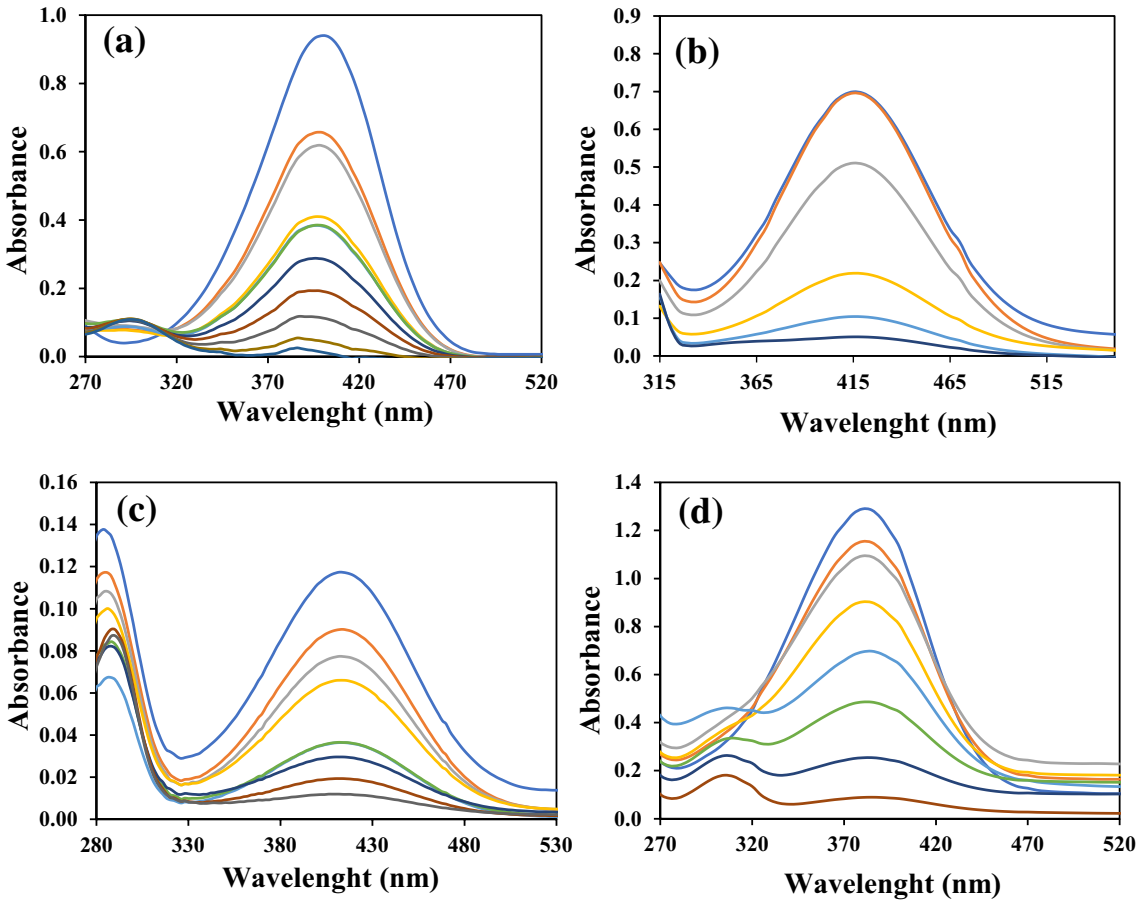

Fig. 6 UV–Vis Spectra for the reduction of **a** 4-NP, **b** 2-NP, **c** 2-NA, and **d** 4-NA catalyzed by Co-p(NIPAM-co-AMPS) nanocomposite

experimental purposes, concentration terms in the Eq. (3) can be replaced with absorbance terms, and the Eq. (3) was modified to Eq. (4).

$$\ln \frac{A_t}{A_o} = -k_{app}t \tag{4}$$

Figure 7a shows the pseudo first order plots for the reduction of all the four nitro compounds. According to Eq. (4), the k_{app} is equal to the slope of the corresponding plot and it

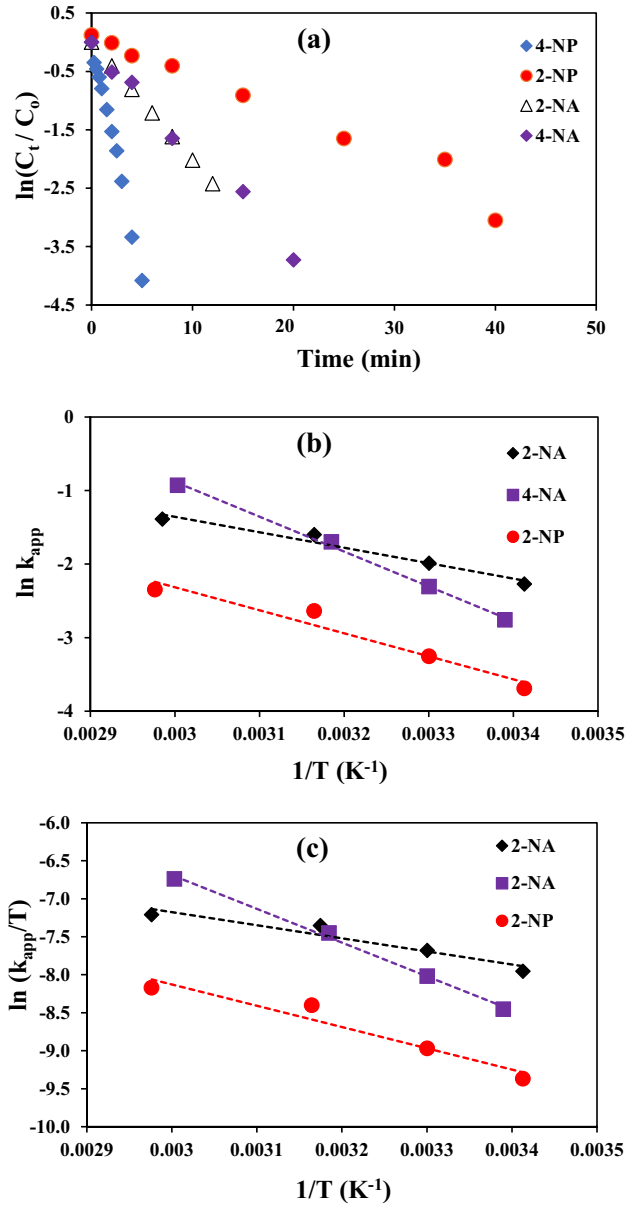

Fig. 7 **a** pseudo first order plots for the reduction of 4-NP, 2-NP, 2-NA, and 4-NA. **b** Arrhenius plots for the determination of activation energy of 2-NA, 4-NA, and 2-NP. **c** Eyring plots for the determination of activation enthalpy and entropy changes

was found 0.56, 0.04, 0.15, and 0.10 for 4-NP, 2-NP, 2-NA, and 4-NA, respectively.

Activation energy, enthalpy, and entropy for the reduction reactions of nitro compounds were calculated by carrying reduction reactions at different temperatures ranging from 20 °C to 60 °C. Activation energy was evaluated by plotting lnk vs 1/T in accordance with Arrhenius Eq. (5) as shown in Fig. 7b, while enthalpy and entropy change was estimated from the slope of ln(k/T) vs 1/T graphs which are shown in Fig. 7c according to Eyring Eq. (6).

$$lnk = lnA - \frac{E_a}{RT} \tag{5}$$

$$\ln \frac{k}{T} = \ln(\frac{k_B}{h}) + \frac{\Delta S^{\#}}{R} - \frac{\Delta H^{\#}}{RT} \tag{6}$$

Activation parameters for the reduction reaction of 4-nitrophenol, 2-nitrophenol, 4-nitroaniline and 2-nitroaniline are summed-up in Table 1. The positive values of enthalpy in activation process represents that the activation process was endothermic. Since, molecules of the reactants need energy to reach the activation state, so the positive value of activation enthalpy change represents the formation of activated complex was carried out by absorption of energy. On the other hand, activation enthalpy change was found negative for all reactions representing the decrease in disorderness owing to ordered arrangement of reactants in activated complex as compared to their random arrangement before the formation of activated complex. So, both the activation enthalpy and entropy changes of all the examined reactions reflect the feasibility of the formation of activated complex in these reactions and hence the occurrence of these reactions as well. The activation energy was found to increase in the order of 2NA < 2NP < 4-NA < 4NP. Generally, it is assumed that a reaction with lower activation energy should proceed faster. Therefore, it could be expected that rate of reactions should be in opposite order of their activation energies. However, it was not found in the present case as k_{app} was found to increase in the order of 2-NP < 4-NA < 2-NA < 4-NP. The highest value of k_{app} for 4-NP represents that either of the collision frequency of the reactants, adsorption of reactants and desorption of the

Table 1 Activation parameters for the reduction reaction of 4-nitrophenol, 2-nitrophenol, 4-nitroaniline and 2-nitroaniline

Reactant	E_a (kJ/mol)	$\Delta S^{\#}$ (J/mol.K)	$\Delta H^{\#}$ (kJ/mol)
2-Nitroaniline	17.46	− 214.33	14.29
4-Nitroaniline	39.40	− 142.55	36.87
2-Nitrophenol	26.01	− 195.29	23.28
4-Nitrophenol	60.59	–	–

product or all these parameters were more favourable for the reduction 4-NP due to specificity of active sites of the catalyst. Figure 8 shows the proposed Langmuir Hinshelwood mechanism for the reduction of 4-NP at the surface of Co nanoparticle [55]. The reaction takes place at the surface of Co nanoparticles fabricated in hydrogel network. The reducing agent $NaBH_4$ produces strong nucleophile (BH_4^-) in water which gives electron to surface of catalyst resulting in the formation of hydride ion. The hydride ions then react with proton (H^+) provided by water to produce molecular hydrogen molecules (H_2). The hydrogen molecules are adsorbed at the surface of Co nanoparticles. The H_2 molecules are converted into active hydrogen atoms by absorption of electron pair in its antibonding orbitals which remain adsorbed at the surface of Co nanoparticles. The active hydrogen atoms then attack at the nitro group of 4-NP and convert it to 4-AP via formation of intermediates containing nitroso (–NO) and hydroxylamino group (–NHOH) as shown by the structural formulas on surface of Co nanoparticles in Fig. 8. When 4-AP is prepared at the surface of Co nanoparticles, it is desorbed from the surface and in this way surface of the nanoparticle is regenerated for further action.

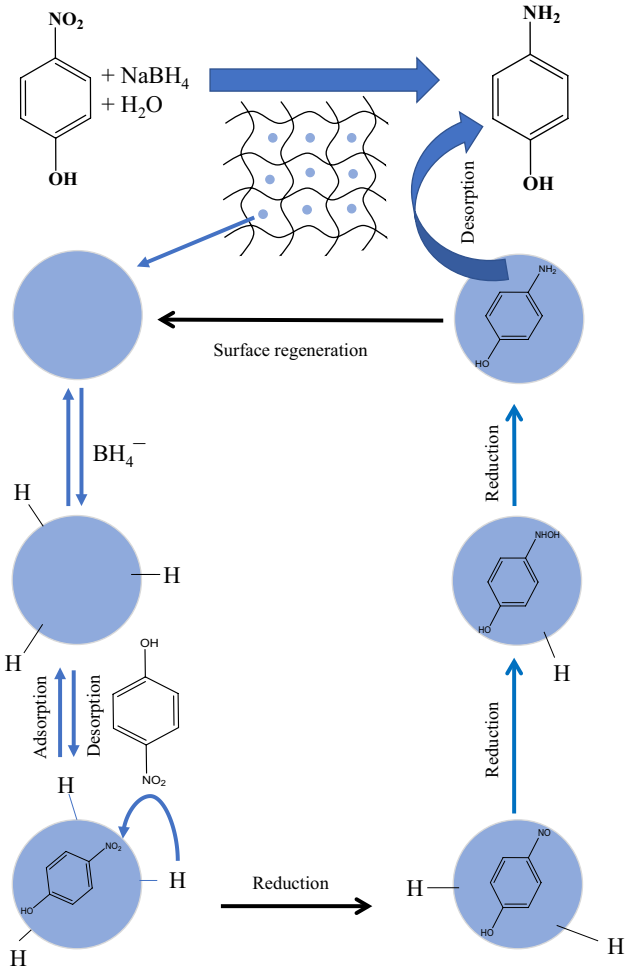

Fig. 8 Langmuir Hinshelwood mechanism for reduction of 4-NP on the surface of Co nanoparticles fabricated in p(NIPAM-co-AMPS) hydroge

To testify the recycling of the catalytic system, the prepared Co-p(AMPS-co-NIPAM) hydrogel composite catalyst, employed in the reaction medium for the reduction of 4-NP, was isolated by filtration through plankton cloth filter, washed with deionized water and applied as catalyst again for the same reaction, under similar reaction parameters. The process was continued for five consecutive cycles. Percent activity of the catalyst and percent conversion of the reactants in recycling process were measured by Eq. (7) and (8), respectively.

$$\%Activity = \frac{k_{app}(i)}{k_{app}(1)} \times 100 \tag{7}$$

$$\%Conversion = \frac{C_f}{C_i} \times 100 \tag{8}$$

where, $k_{app}(1)$ is the k_{app} for the first cycle and $k_{app}(i)$ is k_{app} for any cycle while C_f and C_i are final and initial concentration of reactant in every cycle. The corresponding results are displayed in Fig. 9. The results illustrate that catalytic activity was gradually decreased to 32% in the fifth cycle, however, almost 100% of the available 4-NP was reduced in every cycle. After every successive use, the observed decrease in catalytic activity may happen due to poisoning of the surface of catalysts or oxidation or loss of some Co nanoparticles, which act as catalyst, from Co-p(NIPAM-co-AMPS) hydrogel composite.

4 Conclusions

Synthesis of p(NIPAM-co-AMPS) hydrogel with almost equivalent mesh sizes and homogenous distribution of the functional groups of both the monomers was successfully accomplished by a very simple free radical polymerization method at ambient conditions. The prepared p(NIPAM-co-AMPS) hydrogel subsequently served as a reactor and stabilizing medium for the in-situ fabrication of catalytically active cobalt nanoparticles. The cobalt nanoparticles were found free of agglomerates with an average diameter of 25 nm. An increase in thermal stability of the prepared hydrogel was observed after in-situ fabrication of cobalt nanoparticles. The synthesized Co-p(NIPAM-co-AMPS) hydrogel composite system exhibited very good catalytic activity in the reduction of nitro compounds including 4-NP, 2-NP, 2-NA, and 4-NA with corresponding reduction rates of 0.56, 0.04, 0.15, and 0.10, respectively. A gradual

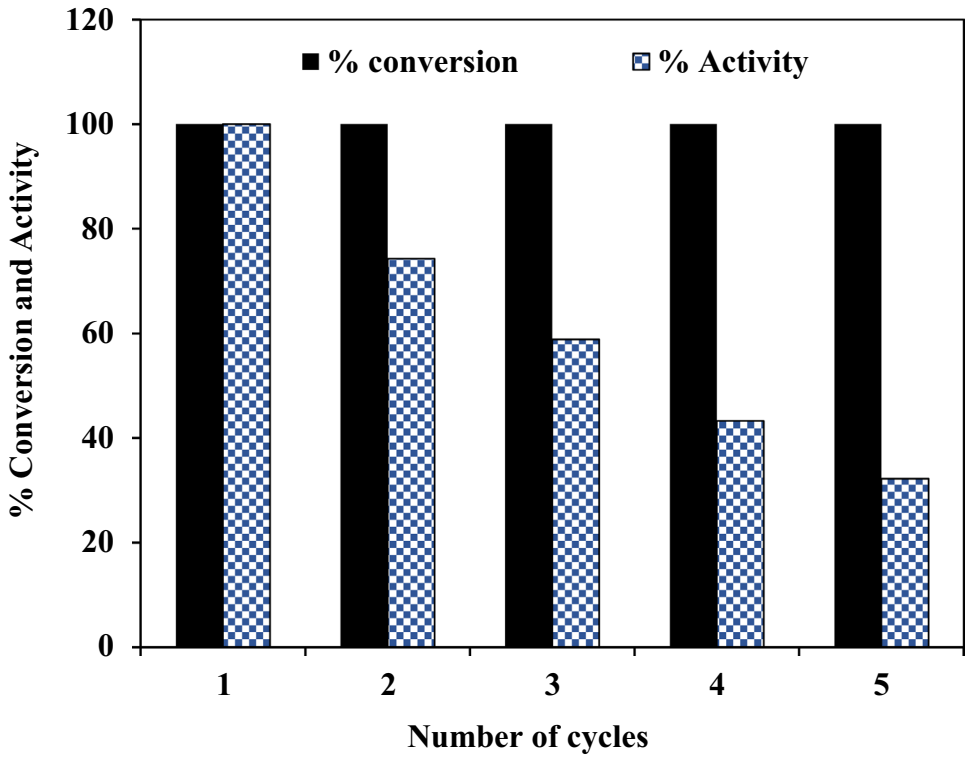

Fig. 9 Percent conversion of 4-NP and percent activity of Co-p(NIPAM-co-AMPS) as a function of cycle number in recycling process

decrease in catalytic activity to 32% was observed in fifth consecutive cycle during the reduction of 4-NP however, almost 100% of the reactant was converted into the product in every cycle.

Funding Financial support from Higher Education Commission of Pakistan via research project No. 21-1844/SRGP/R&D/HEC/2018 is highly appreciated by Muhammad Ajmal.

References

1. L. Belmonte, S.S. Mansy, Elements **12**, 413 (2016)
2. D.I. Sharapa, D.E. Doronkin, F. Studt, J.-D. Grunwaldt, S. Behrens, Adv. Mater. **31**, 1807381 (2019)
3. F. Bibi, M. Ajmal, F. Naseer, Z.H. Farooqi, M. Siddiq, Int. J. Environ. Sci. Technol. **15**, 863 (2018)
4. Z.H. Farooqi, K. Naseem, R. Begum, R.A. Ijaz, J. Inorg. Organomet. Polym. Mater. **25**, 1554 (2015)
5. A.M. Ealias, M. Saravanakumar, IOP Conf. Ser.: Mater. Sci. Eng. **263**, 032019 (2017)
6. H. Kumar, N. Venkatesh, H. Bhowmik, A. Kuila, Biomed. J. Sci. & Tech. Res. **4**, 3765 (2018)
7. Z. Dong, X. Le, X. Li, W. Zhang, C. Dong, J. Ma, Appl. Catal. B-Environ. **158–159**, 129 (2014)
8. Z.-J. Jiang, C.-Y. Liu, L.-W. Sun, J. Phys. Chem. B **109**, 1730 (2005)
9. S. Daripa, R. Verma, D. Guin, C. Chakraborty, K. Awasthi, B.K. Kuila, Langmuir **37**, 2445 (2021)
10. R.K. Narayanan, S.J. Devaki, Ind. Eng. Chem. Res. **54**, 1197 (2015)
11. S. Hecht, J.M.J. Fréchet, Angew. Chem. Int. Ed. **40**, 74 (2005)
12. E. Murugan, J.N. Jebaranjitham, Chem. Eng. J. **259**, 266 (2015)
13. G. Sharma, M. Ballauff, Macromol. Rapid Commun. **25**, 547 (2004)
14. T. Jiao, H. Guo, Q. Zhang, Q. Peng, Y. Tang, X. Yan, B. Li, Sci. Rep.-Uk **5**, 1 (2015)
15. J.-H. Kim, T.R. Lee, Chem. Mater. **16**, 3647 (2004)
16. X. Li, F. Dong, L. Zhang, Q. Xu, X. Zhu, S. Liang, L. Hu, H. Xie, Chem. Eng. J. **372**, 516 (2019)
17. F. Naseer, M. Ajmal, F. Bibi, Z.H. Farooqi, M. Siddiq, Polym. Compos. **39**, 3187 (2018)
18. R.E. Rivero, M.A. Molina, C.R. Rivarola, C.A. Barbero, Sens. Actuators B-Chem. **190**, 270 (2014)
19. J.-S. Shen, Y.-L. Chen, J.-L. Huang, J.-D. Chen, C. Zhao, Y.-Q. Zheng, T. Yu, Y. Yang, H.-W. Zhang, Soft Matter **9**, 2017 (2013)
20. N. Chowdhury, Solaiman, C.K. Roy, S.H. Firoz, T. Foyez, A.B. Imran, ACS Omega **6**, 836 (2021)
21. M. Ghorbanloo, P. Nazari, J. Porous Mat. **27**, 37 (2020)
22. N. Sahiner, Prog. Polym. Sci. **38**, 1329 (2013)
23. L. Ai, J. Jiang, Bioresour. Technol. **132**, 374 (2013)
24. P. Ilgin, O. Ozay, H. Ozay, Appl. Catal. B-Environ. **241**, 415 (2019)
25. G. Marcelo, M. López-González, F. Mendicuti, M.P. Tarazona, M. Valiente, Macromolecules **47**, 6028 (2014)
26. L.A. Shah, A. Haleem, M. Sayed, M. Siddiq, Biochem. Pharmacol. **4**, 3492 (2016)
27. S. ur Rehman, A.R. Khan, A. Shah, A. Badshah, M. Siddiq, Colloids Surf. A **520**, 826 (2017)
28. S. Wu, J. Dzubiella, J. Kaiser, M. Drechsler, X. Guo, M. Ballauff, Y. Lu, Angew. Chem. Int. Ed. **51**, 2229 (2012)
29. S. Ashraf, R. Begum, R. Rehan, W. Wu, Z.H. Farooqi, J. Inorg. Organomet. Polym. Mater. **28**, 1872–1884 (2018)
30. R. Begum, Z.H. Farooqi, E. Ahmed, K. Naseem, S. Ashraf, A. Sharif, R. Rehan, Appl. Organomet. Chem. **31**, 1 (2017)

31. Z.H. Farooqi, S.R. Khan, T. Hussain, R. Begum, K. Ejaz, S. Majeed, M. Ajmal, F. Kanwal, M. Siddiq, Korean J. Chem. Eng. **31**, 1674 (2014)
32. Z.H. Farooqi, K. Naseem, A. Ijaz, R. Begum, J. Polym. Eng. **36**, 87 (2016)
33. Y.-Q. Ma, J.-Z. Yi, L.-M. Zhang, J. Macromol. Sci. Part A **46**, 643 (2009)
34. Z. Cheng, J. Liao, B. He, F. Zhang, F. Zhang, X. Huang, L. Zhou, A.C.S. Sustain, Chem. Eng. **3**, 1677 (2015)
35. R. Wang, X. Jiang, B. Yu, J. Yin, Soft Matter **7**, 8619 (2011)
36. Y. Mei, Y. Lu, F. Polzer, M. Ballauff, M. Drechsler, Chem. Mater. **19**, 1062 (2007)
37. Z.H. Farooqi, R. Khalid, R. Begum, U. Farooq, Q. Wu, W. Wu, M. Ajmal, A. Irfan, K. Naseem, Environ. Technol. **40**, 2027 (2019)
38. Z.H. Farooqi, R. Begum, K. Naseem, U. Rubab, M. Usman, A. Khan, A. Ijaz, Russ. J. Phys. Chem. A **90**, 2600 (2016)
39. Z.H. Farooqi, Z. Butt, R. Begum, S.R. Khan, A. Sharif, E. Ahmed, Mater. Sci.-Poland **33**, 627 (2015)
40. Z.H. Farooqi, S. Iqbal, S.R. Khan, F. Kanwal, R. Begum, E-Polymers **14**, 313 (2014)
41. J. Khan, M. Siddiq, B. Akram, M.A. Ashraf, Arab J. Chem. **11**, 897 (2018)
42. Y. Dong, Y. Ma, T. Zhai, F. Shen, Y. Zeng, H. Fu, J. Yao, Macromol. Rapid Commun. **28**, 2339 (2007)
43. M. Ajmal, Z.H. Farooqi, M. Siddiq, Korean J. Chem. Eng. **30**, 2030 (2013)
44. A.R. Khare, N.A. Peppas, Biomaterials **16**, 559 (1995)
45. A. Haleem, J. Chen, X.-X. Guo, J.-Y. Wang, H.-J. Li, P.-Y. Li, S.-Q. Chen, W.-D. He, Polymer **193**, 122352 (2020)
46. K.R. Shoueir, A.M. Atta, A.A. Sarhan, M.A. Akl, Environ. Technol. **38**, 967 (2017)
47. N. Habeb, T.N. Al-Sabha, Pak. J. Anal. Environ. Chem. **12**, 68 (2011)
48. M. Aamir, M. Farooq, J. Ambreen, N. Ahmad, M. Iqbal, A. Haleem, S. Saeed, A. Shah, M. Siddiq, J. Environ. Chem. Eng. **7**, 103280 (2019)
49. H. Naeem, M. Ajmal, R.B. Qureshi, S.T. Muntha, M. Farooq, M. Siddiq, J. Environ. Manag. **230**, 199 (2019)
50. M. Ajmal, S. Demirci, M. Siddiq, N. Aktas, N. Sahiner, New J. Chem. **40**, 1485 (2016)
51. J. Feng, D. Fan, Q. Wang, L. Ma, W. Wei, J. Xie, J. Zhu, Colloids Surf. A **520**, 743 (2017)
52. R. Begum, J. Najeeb, G. Ahmad, W. Wu, A. Irfan, A.G. Al-Sehemi, Z.H. Farooqi, React. Funct. Polym. **132**, 89 (2018)
53. S.R. Khan, Z.H. Farooqi, M. Ajmal, M. Siddiq, A. Khan, J. Dispers. Sci. Technol. **34**, 1324 (2013)
54. M. Ajmal, M. Siddiq, H. Al-Lohedan, N. Sahiner, RSC Adv. **4**, 59562 (2014)
55. M. Ajmal, F. Aftab, I. Bibi, M. Iqbal, J. Ambreen, H.B. Ahmad, N. Akhtar, A. Haleem, M. Siddiq, J. Porous Mater. **26**, 281 (2019)